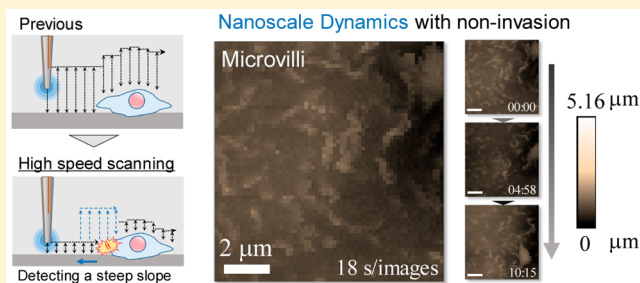


## High Speed Scanning Ion Conductance Microscopy for Quantitative Analysis of Nanoscale Dynamics of Microvilli

Hiroki Ida,<sup>†</sup> Yasufumi Takahashi,<sup>\*,‡,§,||</sup> Akichika Kumatani,<sup>†,||</sup> Hitoshi Shiku,<sup>⊥</sup> and Tomokazu Matsue<sup>\*,†,||</sup><sup>†</sup>Graduate School of Environmental Studies, Tohoku University, Sendai, Miyagi 980-8576, Japan<sup>‡</sup>Division of Electrical Engineering and Computer Science, Kakuma-machi, Kanazawa University, Kanazawa 920-1192, Japan<sup>§</sup>Precursory Research for Embryonic Science and Technology (PRESTO), Japan Science and Technology Agency (JST), Saitama 332-0012, Japan<sup>||</sup>Advanced Institute for Material Research (AIMR), Tohoku University, Sendai, Miyagi 980-8576, Japan<sup>⊥</sup>Department of Applied Chemistry, Graduate School of Engineering, Tohoku University, Sendai 980-8579, Japan

## S Supporting Information

**ABSTRACT:** Observation of nanoscale structure dynamics on cell surfaces is essential to understanding cell functions. Hopping-mode scanning ion conductance microscopy (SICM) was used to visualize the topography of fragile convoluted nanoscale structures on cell surfaces under noninvasive conditions. However, conventional hopping mode SICM does not have sufficient temporal resolution to observe cell-surface dynamics in situ because of the additional time required for performing vertical probe movements of the nanopipette. Here, we introduce a new scanning algorithm for high speed SICM measurements using low capacitance and high-resonance-frequency piezo stages. As a result, a topographic image is taken within 18 s with a  $64 \times 64$  pixel resolution at  $10 \times 10 \mu\text{m}$ . The high speed SICM is applied to the characterization of microvilli dynamics on surfaces, which shows clear structural changes after the epidermal growth factor stimulation.



Microvilli are submicrometric membrane protrusions on epithelial cells mainly comprising actin fiber bundles built on the cell cortex. Microvilli were originally considered static structures that increase the membrane surface area.<sup>1</sup> However, it was recently reported that microvilli have continuous cell functions involved in processes such as  $\text{Ca}^{2+}$  signaling, cell migration,<sup>1</sup> and tension buffering.<sup>2</sup> Furthermore, lateral movements<sup>3</sup> and formation/deformation<sup>4</sup> of microvilli on cell surfaces were found to proceed within a few minutes. Thus, continuous-imaging techniques are required for visualizing microvilli dynamics to investigate the relationship between cell surface morphology and cell function.

Several techniques exist for visualizing microvilli. For example, fluorescent microscopy has been widely used to visualize microvilli by labeled ERM (ezrin/radixin/moesin) proteins.<sup>3</sup> In addition, light-sheet microscopy has been applied to visualize three-dimensional structures as  $z$ -stack images.<sup>2</sup> However, the spatial resolution is not sufficient to observe structural changes at the nanoscale. Alternatively, electron microscopy can be used to visualize surface structures at the nanoscale,<sup>5</sup> but it can only be used to observe cell structures from immobilized cells due to the vacuum condition. To overcome these issues, scanning probe microscopy (SPM) has been used for the evaluation of the various surface properties

with nanoscale resolution.<sup>6–8</sup> In particular, atomic force microscopy (AFM) can be used to observe most cell functions at the nanoscale with high spatiotemporal resolution, and in some cases, it allows for their measurement in solution.<sup>9–11</sup> However, one of the major problems in AFM observation is the probe–sample contact (typically 20 pN to the surface by conventional AFM tip), causing damage to the cell surface. As a result, AFM is not suitable for imaging fragile micro/nanoscale microvilli, which respond to stress less than  $10 \text{ nN}/\text{cm}^2$  ( $10^{-8} \text{ pN}/\text{nm}^2$ ).<sup>12</sup> Therefore, noninvasive imaging techniques are required to visualize cell surface topography at the nanoscale.

Scanning ion conductance microscopy (SICM) is the most suitable method to visualize the fragile and soft materials such as those on the cell surface.<sup>13–20</sup> SICM detects an ion current as a feedback signal for measuring topography obtained through a glass nanopipette filled with electrolyte solution. When the nanopipette approaches the sample, the ion current decreases because the ionic flow is blocked at the top of the nanopipettes. Therefore, SICM is recognized as a noncontact and nonlabeling technique for cell-surface nanoscale-structure

Received: February 15, 2017

Accepted: May 8, 2017

Published: May 8, 2017



imaging.<sup>21</sup> Various scanning methods and algorithms have been developed to improve the temporal resolution for imaging.<sup>22–27</sup> Shevchuk et al. developed modulation-mode SICM to visualize cell-surface protein dynamics.<sup>28</sup> The temporal resolution achieved through this method was 50 s at  $7 \times 7 \mu\text{m}$ .<sup>4</sup> The modulation mode is unsuitable for imaging samples with steep slopes, e.g., neuron and stereocilia, because the nanopipette–sample distance is always maintained constant during scanning. To image a convoluted cell surface, Novak et al. developed hopping-mode SICM.<sup>29</sup> In this mode, the probe is approached and withdrawn at all measurement points; therefore, the hopping mode requires more scanning time compared to the conventional scanning mode. These researchers introduced prescanning to optimize the hopping amplitude and the image pixel size. However, in prescanning, to avoid collision between the nanopipette and the sample during lateral movements in the  $x$ -/ $y$ -axes, the withdrawal amplitude should be sufficiently large.

Improvement of the scanning speed of the hopping-mode SICM is the most important issue in visualizing real cell-surface dynamics. Shevchuk et al. installed a brake booster to improve the approaching speed by avoiding the nanopipette–sample contact due to the latency-dependent overshoot of the Z-piezo stage.<sup>30</sup> The brake booster combines a wide-range Z-piezo stage with a fast-moving Z-piezo stage to avoid contact. These researchers achieved fast scanning with 15 s per frame with  $32 \times 32$  pixels and visualized a rapid endocytosis process.<sup>30,31</sup> However, the temporal resolution of the hopping-mode SICM can be improved further. Currently, the hopping mode requires unnecessary and time-consuming vertical probe movements during approach/withdraw of the nanopipette to/from the sample. Therefore, we developed a new algorithm for optimizing the hopping amplitude during scanning to minimize these unnecessary movements. Typically, the hopping amplitudes were defined at 500 nm and  $3 \mu\text{m}$  at the flat and rough areas, respectively. We also selected a small-capacity Z-piezo stage to improve the temporal resolution in revealing the nanoscale dynamics of microvilli.

## EXPERIMENTAL SECTION

**Cell Preparation.** A431 cells (Cell Resource Center for Biomedical Research, Institute of Development, Aging and Cancer Tohoku University) were cultured in 2 mL Roswell Park Memorial Institute (RPMI) 1640 medium (Gibco) supplemented with 10% fetal bovine serum (FBS) and 1% penicillin streptomycin (Gibco). The cells were incubated at  $37^\circ\text{C}$  with 5%  $\text{CO}_2$  and measured 2–4 days after seeding. Then, the culture medium was changed gently to the Leibovitz's L-15 medium (Gibco).<sup>30</sup> All SICM measurements were performed under ambient air conditions.

**SICM Instrumentation.** The SICM setup has been described in our previous reports.<sup>32,33</sup> Overall SICM system with the specification of hardware components were illustrated in Figure S1. The ionic current was measured using a current amplifier (Axon Instruments, MultiClamp700B) with a feedback resistor of  $500 \text{ M}\Omega$  and a low-pass filter at 1–3 kHz through the head stage. The probe was put close to the sample using a stepping motor (SURUGA SEIKI, C7214-9015) to control the Z-piezo stage (Nano Control, PS1H45-012U). The stepping motor with Z-piezo stage was implemented on a manual operated XYZ manipulator (SURUGA SEIKI, BSS76–60C) with a travel range of  $\pm 6.5 \text{ mm}$ . The precise probe position was controlled by XY- and Z-piezo stages. The

scanning algorithms were controlled by a program written using LabVIEW2014 (National Instruments) in our laboratory. The field-programmable gate array (National Instruments, NI PCIe-7841R) was compiled using our developed programs; the measurement signals were corrected, and all equipment was controlled. The FPGA board was able to respond to up to 200 kS/s as analog inputs and 1 MS/s as analog outputs and 16-bit resolution, respectively. The measurement part of this system was constructed on an optical microscope (Nikon, TE2000-U) on an antivibration table.

**SICM Imaging on Living Cell Surface.** The glass nanopipettes (aperture radius: 50–100 nm) were fabricated from borosilicate glass capillary (GC100F-15, Harvard Apparatus) using a  $\text{CO}_2$  laser puller (Model P-2000, Sutter Instruments). The nanopipettes were used as probes for SICM; they were filled with the L-15 medium, and Ag/AgCl electrodes were inserted into them. The probe was then connected to the head stage of the current amplifier. The applied voltage (0.2 V) made an ionic flow through the tip as a feedback signal. To avoid contact, the probe was approached to the point where the ionic current decreased to the set points and withdrawn from the cell surface after each measurement point.

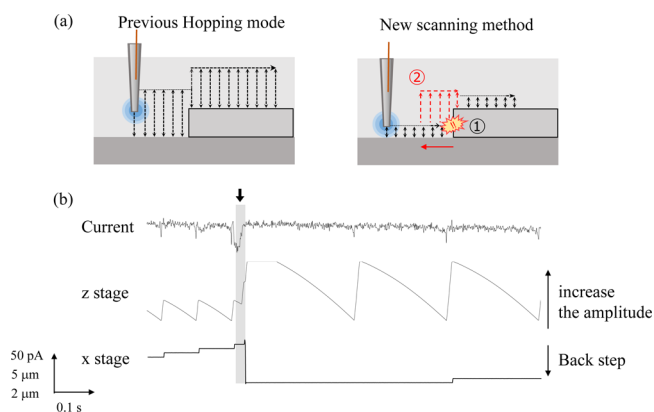


**Figure 1.** Schematic representation of the high speed SICM algorithm. (a) Illustrations of the previous hopping mode and our new scanning method. When the previous system is applied, the SICM probe is withdrawn using the Z-piezo stage with constant height after each measurement points (left). On the other hand, when the new scanning algorithm is applied, the withdrawal amplitude is controlled, as shown on the right. If the probe contacts the sample during lateral movements (1), the probe pulls back to a few steps and increases the withdrawal amplitude to avoid the contact (2). (b) Changes in the ion current and piezo monitor. The arrow indicates the moment then a nanopipette makes contact with a sample (highlighted by gray color).

## RESULTS AND DISCUSSION

To visualize the morphological dynamics of microvilli, we used a small-capacitance and high-resonance-frequency piezo actuator equipped with XY- and Z-piezo stages. The capacitance and resonance frequency of the piezo stages are  $6.8 \mu\text{F}$  (X- and Y-axes) and  $1.4 \mu\text{F}$  (Z-axis), and 2.5 kHz (X, Y-axes) and 6.2 kHz (Z-axis), respectively.<sup>32</sup> These XY- and Z-piezo stages improve the lateral movement (2 ms/step) and the approach (500 nm/ms) and withdraw (1500 nm/ms) speeds. Next, we developed a new algorithm for high speed scanning to optimize the withdrawal length during imaging (Figure 1a). In the new algorithm, the withdrawal distance was set at the lower than the maximum of surface roughness (under  $0.5 \mu\text{m}$ ). In this

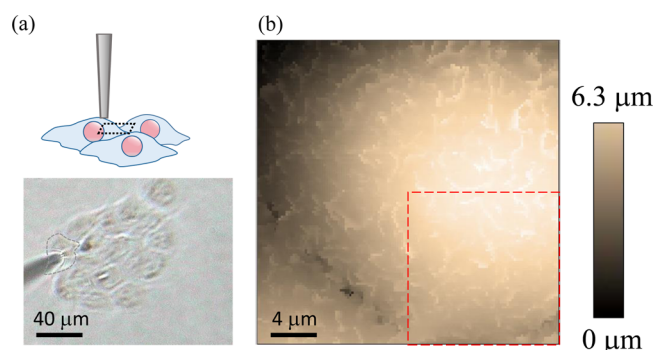


**Figure 2.** SICM topography image of a single surface. (a) Schematic illustration of SICM measurement (upper) and optical microscope image (lower). (b) SICM image of ridge-like microvilli on the A431 cell surface. This image was taken at  $20 \times 20 \mu\text{m}$  with  $128 \times 128$  pixels. The red broken square indicates the continuous imaging area shown in Figure 3.

condition, at a low roughness area, it did not affect the fast scanning. On the other hand, at a high roughness area (over  $0.5 \mu\text{m}$ ), the probe was touched lightly to the sample surface, and then the current decreased during lateral movements. It should be noted that there would be a limitation to scan the sample surface with some floating location in this algorithm, as far as the probe would touch lightly to the sample surface. It is because the probe would have to risk dragging the location by light touching. Also, as long as the sample surface roughness was lower than the limit range of Z-piezo movement ( $12 \mu\text{m}$  in this case), the algorithm was applicable. If the current was decreased up to a set point during lateral movements, the probe recognized it as a steep point. Then, the probe avoided a contact by a step back to a former XY scanning position ( $\sim 10$  steps). After that, the withdrawal distance was increased in steps until the probe overcame the steep point. The algorithm was able to visualize higher steep points as long as they were

within the range of movement of the Z-piezo stage. Therefore, it can handle a steep roughness and rapid morphological variation. The scanning rate was improved owing to a reduction of the unnecessary probe vertical movements at the smooth area. As a result, it allowed us to obtain a topography image in 18 s with  $64 \times 64$  pixels at  $10 \times 10 \mu\text{m}$  for microvilli.

Furthermore, SICM with the newly developed scanning algorithm is applied here for revealing the nanoscale dynamics of microvilli in A431 cells. The SICM image (Figure 2b) shows numerous microvillar constructions on the A431 cell surface. Remarkably, microvilli are less dense, and cell junctions seemed to be loosely conjugated, as compared to those in a previous report.<sup>4</sup> This phenomenon is attributed to a change in the mechanical features of nonconfluent cells in this experiment. Next, we obtain continuous topography images at the red broken square area in Figure 2b with higher temporal resolution. The time-lapse images reveal that microvilli move in various directions (Figure 3a and Movie 1). The movement seems to be related to the reorganization of the cortical actomyosin cytoskeleton by active myosin.<sup>3</sup> Subsequently, the existence and location of microvilli were determined using an adaptive thresholding algorithm (Figure 3a, lower) and analyzed statistically from the obtained diagrams of the distribution of microvilli heights. Figure 3b shows the reconstructed histogram of a microvillus height through SICM image analysis; the median is approximately 180 nm. It is also noted that the height and density of microvilli remain moderately constant (Figures 3c and d), even though the microvilli move often. Importantly, there is no significant change in the density and form of the microvilli during the SICM measurement, indicating that probe scanning does not affect the surface structure of the cells.

To investigate the effect of actin polymerization on microvilli movement, SICM time-lapse topography imaging of microvilli was performed after epithelial growth factor (EGF) stimulation. EGF stimulation significantly proliferates and activates actin

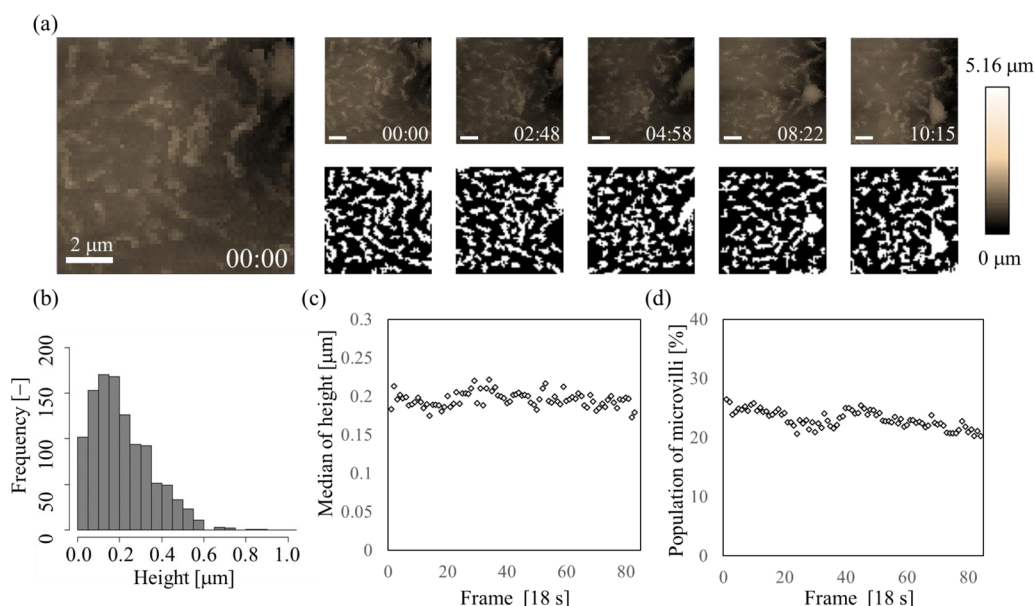


**Figure 3.** Continuous morphological changes of microvilli on a living cell surface. (a) Time-lapse imaging on an A431 cell surface. Topography images appear in the upper part. In the lower part, we see binarized images produced using the adaptive thresholding algorithm to extract the microvilli clearly. (b) Histogram of the extracted microvilli heights. Temporal changes of the median (c) and the proportion (d) of microvilli in the scanning area. All images were taken at  $10 \times 10 \mu\text{m}$  with  $64 \times 64$  pixels.



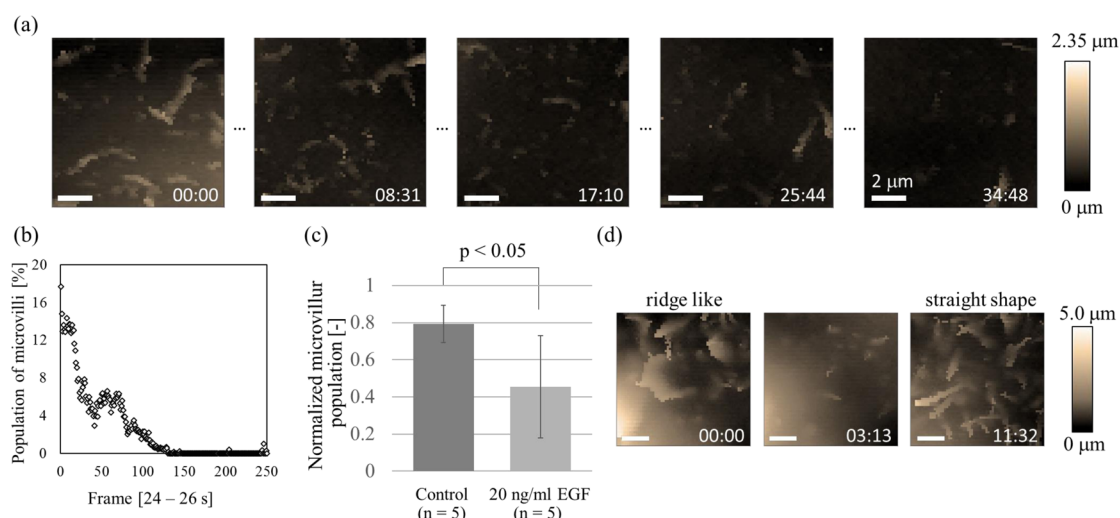


**Figure 4.** Microvilli dynamics after EGF exposure. (a) Time-lapse imaging of a stimulated A431 cell surface after stimulation with a 20 ng/mL EGF. (b) Temporal changes in the population of microvilli within the scanning area. After treatment with a 20 ng/mL EGF, most microvilli disappeared from the cell surface. (c) Population variation of microvilli on the cell surface with  $10 \times 10 \mu\text{m}$  after 20 min from the start of SICM measurements. (d) Microvilli changed their shapes from ridge-like to straight-shaped after treatment with a 100 ng/mL EGF. All images were taken at  $10 \times 10 \mu\text{m}$  with  $64 \times 64$  pixels.

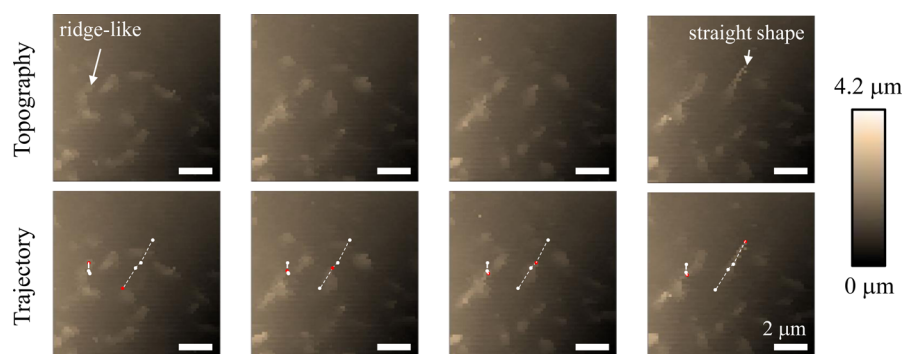


**Figure 5.** Comparison between concurrent ridge-like and straight-shaped microvillus movements. The ridge-like microvillus movement speed is approximately 12 nm/s. On the other hand, the straight-shaped microvillus movement speed is approximately 100 nm/s. All images were taken at  $10 \times 10 \mu\text{m}$  with  $64 \times 64$  pixels.

polymerization.<sup>34,35</sup> Therefore, it is expected to elongate microvilli or increase the amount of microvilli because microvilli would be organized in actin bundles. However, unexpectedly, most microvilli disappear from the cell surface (Figures 4a and b). These results suggest that the elongation or increase in the amount of microvilli is secondary to other actin structural events such as the construction of filopodia and the elongation of stress fibers attending cell migration. It is most likely that microvilli buffer the cell tension by dissolving when the cell migrates.<sup>2</sup>

After disappearance of these microvilli, straight-shaped microvilli appear in some areas (Figure 4d), as Poole et al. reported previously.<sup>36</sup> Notably, the movement speed of straight microvilli is approximately 100 nm/s based on the images, which is greater than those of the ridge-like shapes by approximately 12 nm/s (Figure 5 and Movies 2 and 3). Moreover, it is revealed that the straight microvilli move in one particular direction.

This indicates that the mechanisms of the microvilli framing and the driving forces for straight microvilli are different from those for the ridge-like shapes. This difference is probably caused by the fact that microvilli with straight shape are constructed by a bundle of actomyosin.<sup>37,38</sup> The morphology of

the actomyosin cortex depends on the tension of the microvilli. At low tension, the actomyosin forms a network structure by connecting each actin bundle with myosin. Furthermore, when its tension increases because of the myosin, the network structure changes to that of the stressed fiber form by parallel agglutination. The bundle with the stressed fiber form is straight and unipliable. This is in agreement with the microvilli shapes and movements observed in the SICM images after EGF exposure. Actomyosin movements are derived by myosin activity connecting two actin filaments.<sup>39</sup> The movements of straight microvilli are activated by the parallel connection force of myosin, whereas such a vectorial force may not occur in a network structure with ridge-like shapes. This difference in force can cause a difference in the movement speeds of microvilli with straight and ridge-like shapes.

## CONCLUSION

We developed high speed SICM with a new scanning algorithm for optimization of probe movements using a piezo stage with low capacity and high resonance frequency. Using this high speed SICM, topography images were obtained in 18 s with  $64 \times 64$  pixels at  $10 \times 10 \mu\text{m}$  resolution. The high speed SICM system was applied to the observation and evaluation of

microvilli on cell surfaces. From the SICM images, we measured the movement speeds of straight and ridge-like shapes microvilli at 100 and 12 nm/s, respectively. The microvilli moved in various directions and maintained their density and height in an almost constant manner. Exposure to 20 ng/mL EGF stimulation led to the disappearance of most microvilli from the cell surface and other structural changes within 20 min. This is interpreted in terms of modified mechanical features in the cell. Therefore, this SICM method allows for noninvasive and high speed imaging. The present SICM system is expected to become a powerful tool for revealing morphological changes on single cell surfaces at the nanoscale.

## ■ ASSOCIATED CONTENT

### Supporting Information

The Supporting Information is available free of charge on the ACS Publications website at DOI: [10.1021/acs.analchem.7b00584](https://doi.org/10.1021/acs.analchem.7b00584).

Microvilli dynamics on unstimulated living cell surface (AVI)

Microvilli dynamics on EGF stimulated living cell surface (AVI)

Microvilli dynamics on EGF stimulated living cell surface (AVI)

Experimental details (PDF)

## ■ AUTHOR INFORMATION

### Corresponding Authors

\*E-mail: [yasufumi@se.kanazawa-u.ac.jp](mailto:yasufumi@se.kanazawa-u.ac.jp); Tel: (+81)-076-234-4866.

\*E-mail: [matsue@bioinfo.che.tohoku.ac.jp](mailto:matsue@bioinfo.che.tohoku.ac.jp).

### ORCID

Yasufumi Takahashi: 0000-0003-2834-8300

Akichika Kumatani: 0000-0001-7198-8990

### Notes

The authors declare no competing financial interest.

## ■ ACKNOWLEDGMENTS

This work is supported by Development of Systems and Technology for Advanced Measurement and Analysis from AMED (The Japan Agency for Medical Research and Development)-SENTAN, and ALCA and PREST from the Japan Science and Technology Agency (JST), a Grant-in-Aid for Scientific Research (A) (16H02280), a Grant-in-Aid for Scientific Research (B) (15H03542), a Grant-in-Aid for Young Scientists (A) (15H05422 and 16H06042) from the Japan Society for the Promotion of Science (JSPS) and Nakatani Foundation, Grant-in-Aid for JSPS Research Fellow, and a Grant-in-Aid of Tohoku University Institute for Promoting Graduate Degree Programs Division for Interdisciplinary Advanced Research and Education.

## ■ REFERENCES

- (1) Lange, K. J. *Cell. Physiol.* **2011**, 226, 896–927.
- (2) Planchon, T. A.; Gao, L.; Milkie, D. E.; Davidson, M. W.; Galbraith, J. A.; Galbraith, C. G.; Betzig, E. *Nat. Methods* **2011**, 8, 417–U68.
- (3) Klingner, C.; Cherian, A. V.; Fels, J.; Diesinger, P. M.; Aufschneider, R.; Maghelli, N.; Keil, T.; Beck, G.; Tolic-Norrelykke, I. M.; Bathe, M.; Wedlich-Soldner, R. *J. Cell Biol.* **2014**, 207, 107–121.
- (4) Gorelik, J.; Shevchuk, A. I.; Frolenkov, G. I.; Diakonov, I. A.; Lab, M. J.; Kros, C. J.; Richardson, G. P.; Vodyanoy, I.; Edwards, C. R. W.; Klenerman, D.; Korchev, Y. E. *Proc. Natl. Acad. Sci. U. S. A.* **2003**, 100, 5819–5822.
- (5) Chinkers, M.; McKanna, J. A.; Cohen, S. J. *Cell Biol.* **1979**, 83, 260–265.
- (6) Nadappuram, B. P.; McKelvey, K.; Al Botros, R.; Colburn, A. W.; Unwin, P. R. *Anal. Chem.* **2013**, 85, 8070–8074.
- (7) Nogala, W.; Velmurugan, J.; Mirkin, M. V. *Anal. Chem.* **2012**, 84, 5192–5197.
- (8) Actis, P.; Maalouf, M. M.; Kim, H. J.; Lohith, A.; Vilozny, B.; Seger, R. A.; Pourmand, N. *ACS Nano* **2014**, 8, 546–553.
- (9) Poole, K.; Meder, D.; Simons, K.; Muller, D. *FEBS Lett.* **2004**, 565, 53–58.
- (10) Shibata, M.; Uchihashi, T.; Yamashita, H.; Kandori, H.; Ando, T. *Angew. Chem., Int. Ed.* **2011**, 50, 4410–4413.
- (11) Kodera, N.; Yamamoto, D.; Ishikawa, R.; Ando, T. *Nature* **2010**, 468, 72–76.
- (12) Miura, S.; Sato, K.; Kato-Negishi, M.; Teshima, T.; Takeuchi, S. *Nat. Commun.* **2015**, 6, 8871.
- (13) Hansma, P. K.; Drake, B.; Marti, O.; Gould, S. A. C.; Prater, C. B. *Science* **1989**, 243, 641–643.
- (14) Korchev, Y. E.; Bashford, C. L.; Milovanovic, M.; Vodyanoy, I.; Lab, M. J. *Biophys. J.* **1997**, 73, 653–658.
- (15) Takahashi, Y.; Murakami, Y.; Nagamine, K.; Shiku, H.; Aoyagi, S.; Yasukawa, T.; Kanzaki, M.; Matsue, T. *Phys. Chem. Chem. Phys.* **2010**, 12, 10012–10017.
- (16) Shevchuk, A. I.; Frolenkov, G. I.; Sanchez, D.; James, P. S.; Freedman, N.; Lab, M. J.; Jones, R.; Klenerman, D.; Korchev, Y. E. *Angew. Chem., Int. Ed.* **2006**, 45, 2212–2216.
- (17) Ushiki, T.; Nakajima, M.; Choi, M.; Cho, S. J.; Iwata, F. *Micron* **2012**, 43, 1390–1398.
- (18) Seifert, J.; Rheinlaender, J.; Novak, P.; Korchev, Y. E.; Schaffer, T. E. *Langmuir* **2015**, 31, 6807–6813.
- (19) Adler, J.; Shevchuk, A. I.; Novak, P.; Korchev, Y. E.; Parmryd, I. *Nat. Methods* **2010**, 7, 170–171.
- (20) Takahashi, Y.; Kumatani, A.; Shiku, H.; Matsue, T. *Anal. Chem.* **2017**, 89, 342–357.
- (21) Del Linz, S.; Willman, E.; Caldwell, M.; Klenerman, D.; Fernandez, A.; Moss, G. *Anal. Chem.* **2014**, 86, 2353–2360.
- (22) Momotenko, D.; Byers, J. C.; McKelvey, K.; Kang, M.; Unwin, P. R. *ACS Nano* **2015**, 9, 8942–8952.
- (23) Leo-Macias, A.; Agullo-Pascual, E.; Sanchez-Alonso, J. L.; Keegan, S.; Lin, X. M.; Arcos, T.; Feng Xia, L.; Korchev, Y. E.; Gorelik, J.; Fenyo, D.; Rothenberg, E.; Delmar, M. *Nat. Commun.* **2016**, 7, 1.
- (24) Shevchuk, A.; Tokar, S.; Gopal, S.; Sanchez-Alonso, J. L.; Tarasov, A. I.; Velez-Ortega, A. C.; Chiappini, C.; Rorsman, P.; Stevens, M. M.; Gorelik, J.; Frolenkov, G. I.; Klenerman, D.; Korchev, Y. E. *Biophys. J.* **2016**, 110, 2252–2265.
- (25) Happel, P.; Hoffmann, G.; Mann, S. A.; Dietzel, I. D. *J. Microsc.* **2003**, 212, 144–151.
- (26) Zhukov, A.; Richards, O.; Ostanin, V.; Korchev, Y.; Klenerman, D. *Ultramicroscopy* **2012**, 121, 1–7.
- (27) Momotenko, D.; McKelvey, K.; Kang, M.; Meloni, G. N.; Unwin, P. R. *Anal. Chem.* **2016**, 88 (5), 2838–2846.
- (28) Shevchuk, A. I.; Gorelik, J.; Harding, S. E.; Lab, M. J.; Klenerman, D.; Korchev, Y. E. *Biophys. J.* **2001**, 81, 1759–1764.
- (29) Novak, P.; Li, C.; Shevchuk, A. I.; Stepanyan, R.; Caldwell, M.; Hughes, S.; Smart, T. G.; Gorelik, J.; Ostanin, V. P.; Lab, M. J.; Moss, G. W. J.; Frolenkov, G. I.; Klenerman, D.; Korchev, Y. E. *Nat. Methods* **2009**, 6, 279–281.
- (30) Shevchuk, A. I.; Novak, P.; Taylor, M.; Diakonov, I. A.; Ziyadeh-Isleem, A.; Bitoun, M.; Guicheney, P.; Lab, M. J.; Gorelik, J.; Merrifield, C. J.; Klenerman, D.; Korchev, Y. E. *J. Cell Biol.* **2012**, 197, 499–508.
- (31) Novak, P.; Shevchuk, A.; Ruenaroengsak, P.; Miragoli, M.; Thorley, A. J.; Klenerman, D.; Lab, M. J.; Tetley, T. D.; Gorelik, J.; Korchev, Y. E. *Nano Lett.* **2014**, 14, 1202–1207.

- (32) Takahashi, Y.; Ito, K.; Wang, X. W.; Matsumae, Y.; Komaki, H.; Kumatani, A.; Ino, K.; Shiku, H.; Matsue, T. *Electrochemistry* **2014**, *82*, 331–334.
- (33) Takahashi, Y.; Shevchuk, A. I.; Novak, P.; Murakami, Y.; Shiku, H.; Korchev, Y. E.; Matsue, T. *J. Am. Chem. Soc.* **2010**, *132*, 10118–10126.
- (34) Rijken, P. J.; Hage, W. J.; Henegouwen, P.; Verkleij, A. J.; Boonstra, J. *J. Cell Sci.* **1991**, *100*, 491–499.
- (35) Bolshakova, A.; Magnusson, K. E.; Pinaev, G.; Petukhova, O. *Histochem. Cell Biol.* **2015**, *144*, 223–235.
- (36) Poole, K.; Muller, D. *Br. J. Cancer* **2005**, *92*, 1499–1505.
- (37) Aratyn-Schaus, Y.; Oakes, P. W.; Gardel, M. L. *Mol. Biol. Cell* **2011**, *22*, 1330–1339.
- (38) Blanchoin, L.; Boujemaa-Paterski, R.; Sykes, C.; Plastino, J. *Physiol. Rev.* **2014**, *94*, 235–263.
- (39) Gowrishankar, K.; Ghosh, S.; Saha, S.; Rumamol, C.; Mayor, S.; Rao, M. *Cell* **2012**, *149*, 1353–1367.